

MOMENTUM BALANCE OF A GLASS-PLATE PATCH IN SHALLOW FLOW

O. Eiff, V. Dupuis, M. Trevisson, S. Wunder, D. Hettmann, A. Zygouli (1)
L. Chagot, F. Moulin (2)
B. Murphy, & S. McLelland (3)

(1) KIT, Karlsruhe, Germany, Email: olivier.eiff@kit.edu; victor.dupuis@kit.edu

(2) IMFT, Université de Toulouse, CNRS-INPT-UPS, Toulouse, France, Email: fmoulin@imft.fr

(3) University of Hull, Hull, Great Britain, Email: S.J.McLelland@hull.ac.uk

The resistance to flow of aqueous vegetation patches is a challenge to model due to their complex geometry and topological adaption under hydrodynamic loading. Patches not only influence the water level and mean velocities due to the drag they exert, but they also affect the turbulence and hence the processes such as the sediment deposition and erosion within and around the patch. Existing studies dealing with the interaction of flow and vegetation mostly measured the drag of individual plants or focused on the flow through and above homogeneous canopies. Studies of the flow around and within isolated patches are scarce and restricted to arrays of cylindrical elements. For leafy plants or surrogates there is only limited if any information and understanding of how the flow evolves through and around the plants. In this access project, the aim was to fill this gap via complementary physical lab-scale and numerical experiments of the flow through and around a surrogate leafy vegetation patch. The measurements were also performed around a real plant in the same flow configuration. Here, we focus on the momentum budget based on the measurements around the surrogate plant performed via stereoscopic particle image velocimetry (SPIV).

1. INTRODUCTION

The prediction of flow velocities and water levels during flood events is a challenge due to the need to account for the flow resistance or drag of complex emergent and/or submerged obstacles. The flow resistance due to vegetation patches is particularly difficult to quantify due to their complex geometry and topological change under hydrodynamic loading and seasonal conditions. Vegetation also affect locally the flow field including the turbulence and associated mass transfer processes. The flow resistance and interactions depend on the allometric characteristics of the vegetation patch itself. These are generally described by frontal density, solid volume fraction, leaf area index (LAI), shape and flexibility, with major uncertainties both in their flow-dependent determination and parameterization, necessary for implementation in larger-scale numerical models (Aberle & Järvelä, 2013; Boothroyd et al., 2015; Jalonen et al., 2013; Marjoribanks et.al., 2014).

Existing investigations on the vegetation drag were mostly performed by direct force measurements using the classical one-parameter drag force equation for solid bodies to parameterize the effects of the allometric plant characteristics by modifying the velocity dependence with additional parameters (Aberle & Järvelä; Armanini et al., 2005; Wunder et al., 2011). However, as recent studies on the flow through emergent single vegetation patches (Nicolle & Eames, 2011; Rominger & Nepf, 2011) have shown, the use of such parameterization of the drag force equation is questionable when the plant is significantly penetrated by the flow. To avoid these parametrizations, studies have started to investigate the flow itself around emergent patches constructed by arrayed cylinders, to better characterize the flow pattern and turbulence structures in the wake zone (Tanino & Nepf, 2008; Thomas & McLelland, 2015). In these studies the flow was characterized by instantaneous and local velocity measurements. Yet, most of the local flow investigations did not focus on the question of the drag parametrization but on the morphodynamic processes within and downstream of the emergent patches (Chen et al., 2012; Kim et al., 2016). PIV-measurements around patches have so far only been performed in the wake zone of a single and submerged artificial fractal tree (Bai et al, 2012, 2013). Numerical

(RNG and LES) investigations of the flow field within and around a patch have also been performed and have so far considered emergent arrays of solid cylinders (Chang et al., 2017; Marjoribanks, 2014a, 2014b) or artificial plants (Boothroyd et al, 2015; Stoesser et al., 2010; Zong & Nepf, 2011). In summary, for leafy plants there is still very limited information and understanding of how the flow through them and the resulting drag evolves. This paper proposes to start filling these gaps by performing PIV-measurements around an artificial leafy patch made of glass plates. The PIV measurements were performed in a stereoscopic configuration in order to be able to include the necessary transverse planes as well as the out-of-plane components, necessary for a full momentum balance. The artificial plant meets the allometric characteristics of a real leafy plant. The project also included measurements around a real leafy plant and measurements within the artificial plant. Here, the focus is on the momentum balance of the artificial plant for one flow configuration and includes an analysis of the turbulent flow structure in the near-wake of the patch.

2. EXPERIMENTAL SET-UP

The experiments were performed in the recirculating Total Environment Simulator of Hull University, Great Britain, a glass-walled flume 6 m wide and 10 m long. The effective flume width was symmetrically reduced to a width $B = 3$ m in order to use a side-looking submersible stereo PIV set-up described below. This effective width still enabled to minimize side wall effects in a shallow-water configuration with water depth $h = 20$ cm, while retaining a large enough patch for Reynold number similarity. The patch, consisting of a geometrically ordered structure, designed with 35 vertical glass plates, $t = 1$ mm thin, $l = 4$ cm long and $h_p = 20$ cm high, arranged in a staggered configuration (cf. Figure 1a), was installed in the centre of the flume. The bed of the flume was covered by gravel with mean diameter of $d_g = 2$ cm (cf Figure 1b). The bed was not water-worked but levelled manually to obtain a flat bed. The levelling is expected to lower the roughness. To cover the allometric parameters of a real leafy plant, the design of the geometry (number of plates per base area) met the natural values of solid volume fraction, i.e. porosity ($\phi = 0.98$), and the leaf area index (LAI = 4.0) of a real shrubby willow. The layout of the 35 glass plates spaced at distance $s = 33$ mm apart is given in Figure 2. The patch has a total width $b = 27.3$ cm so that $B/b > 10$ and length $a = 34.2$ cm and was positioned 7 m downstream from a set of grids to homogenize the flow and to reduce inlet turbulence intensities. The coordinate origin is fixed at the middle of the upstream edge of the patch, with x the longitudinal direction, y the transverse and z the vertical directions.



Figure 1. Design of the artificial patch (a), meeting the allometric characteristics of a natural willow plant, installed in the flume (b), and during experiments (c).

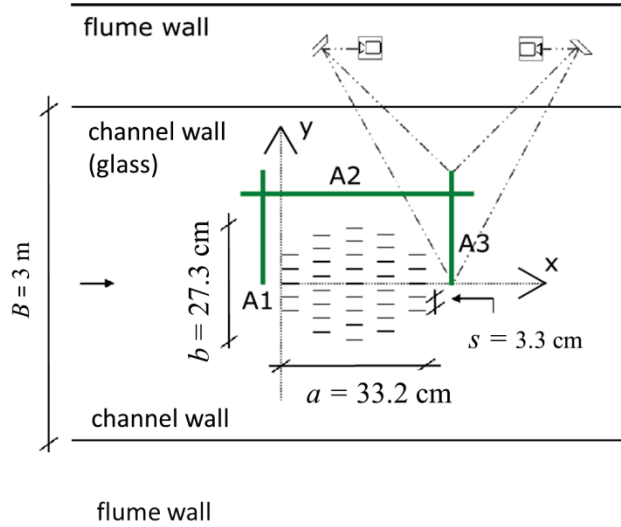


Figure 2. Set-up of the stereoscopic PIV (SPIV). The green lines refer to SPIV measurement planes. Not to scale.

The flow field around the patch was characterized by stereoscopic 2D-3C PIV measurements in two transverse vertical planes and a longitudinal plane (Figure 2). The transverse planes were positioned upstream of the patch 3.4 cm upstream to the first row of glass sheets ($x = -3.4$ cm and 3.4 cm downstream of the patch last row of glass plates ($x = 36.6$ cm). The longitudinal plane was positioned at $y = 25$ cm. On the basis of upstream ADV measurements, it can be reasonably assumed that the flow field behaves symmetrically with respect to the centreline in flow direction. Measurements were performed for relative submergence of plant-height to water-depth $h_p/h = 1$, a bulk flow velocity of $U_b = 0.3$ m/s and a flow depth of $h = 0.2$ m. The Reynolds-number of the channel flow is $\text{Re}_f = U_b h / \nu = 6.0 \times 10^4$ and the leaf Reynolds-number $\text{Re}_l = U_b l / \nu = 1.2 \times 10^4$. The transverse plane measurements were also performed with the patch.

The instrumentation consisted of a 2×120 mJ pulsed laser from Dantec Dynamics producing a 10 mm thick laser sheet synchronized with two CMOS cameras with a resolution of 2320 pixels \times 1726 pixels and mounted with motorized 65 mm lenses. The cameras were positioned in a 1.5 m long underwater-torpedo from Dantec in the side-channel which recorded the images via adjustable mirrors. The seeding used was PLASCOAT TALISMAN 20 with a mean density of $\rho = 0.99$ g/cm³ and a particle size of about 180 μm . To converge statistically, 5000 image pairs with a sampling rate of 4 Hz were collected for each camera and each measurement plane. The data was processed with the Davis software from Lavision.

3. RESULTS AND DISCUSSION

Comparison of the longitudinal velocity contours without the patch in the two transverse planes 1 and 3 shown in Figure 3a-b suggests that the flow was developed. Also, the turbulent shear stress $-\rho u' w'(z)$ (not shown) can be seen to be essentially linear except near the bed, suggesting developed and 2D flow. Yet, the velocity contours also reveal relatively strong lateral variations. This non-uniformity does not appear to be associated with secondary circulations but with non-uniformity at the inlet. The friction velocity evaluated from the linear extrapolation of the fitted turbulent shear stress down to the top of the gravel bed yielded a value of 2.5 cm/s. The velocity profiles were fitted with the logarithmic law with a van Karman constant of 0.41 and yielded an equivalent sand-roughness of the manually-levelled gravel bed $k_s = 3$ mm, resulting in $k_s^+ \geq 70$, i.e. fully rough flow.

Figure 4a-b show the longitudinal velocity component with the patch in the upstream and downstream transverse planes, respectively. In the downstream plane, vertical bar-like structures of lower velocity can be identified which are clearly the signatures of the upstream glass plates. This suggests that the individual wakes of the plates have not merged. Also, except close to the ground, the wake velocities are relatively uniform in strength. The non-uniformity of the flow outside of the wake region is relatively well correlated with the no-patch flows shown in Figure 2 and therefore do not represent a wake or patch effect.

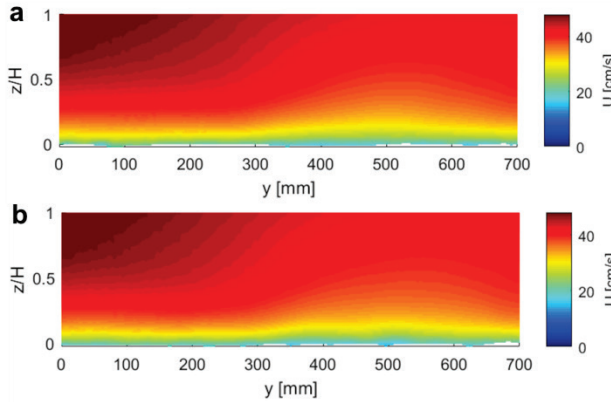


Figure 3. Gravel bed flow without patch. Contour plot of the longitudinal velocity at $x = -3.4$ cm (a) and at $x = 36.6$ cm (b).

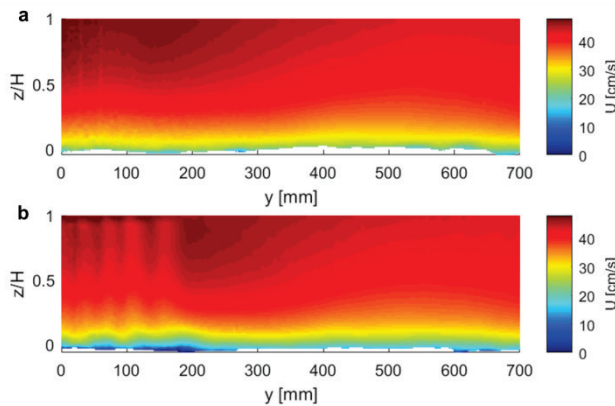


Figure 4. Gravel bed flow with patch. Contour plot of the longitudinal velocity upstream of the patch at $x = -3.4$ cm (a) and downstream at $x = 36.6$ cm (b).

Figure 5 shows, from measurement plane A3 downstream of the patch, the lateral profiles of the time-averaged longitudinal velocity \bar{u} , the time averaged lateral velocity \bar{v} , the normal turbulent stress $\rho \bar{u}^2$, the lateral turbulent shear stress $\rho \bar{u}'\bar{v}'$, all at $z/h = 0.39$ and $z/h = 0.88$. The green lines show the position of minimum \bar{u} , i.e. the centre of the wakes. The black solid and dashed lines indicate the position of the glass blades. The black solid lines correspond to positions for three rows of blades (rows 1, 3, 5), while the black dashed lines to two rows (2, 3). For $y = 0$ the green and black lines overlap. For higher y 's, the separation increases with increasing y suggesting that the wakes are deviating. Interestingly, rows 2 and 3 (dashed lines) do not appear with minimum \bar{u} signature. There are only five green lines or \bar{u} minima, as seen in Figure 4b. Minimum \bar{u} do not quite correspond to $\bar{v} = 0$ which again suggests a deviation of the wakes. It should also be noted that the mean velocity profiles are in phase at the two heights plotted, again in agreement with the columnar iso-contours seen in Figure 4b. The normal stress does not reveal an evident phase relationship and is in fact slightly lower in the wake than in the free stream, suggesting that the blades are reducing the turbulent kinetic energy of the flow. The lateral turbulent shear stress again reveals a strong variation in the wake. Maximum negative values are expected at the strongest positive gradient of $d\bar{u}/dy$, which the profiles mostly corroborate, again suggesting that the wakes generated by the separating boundary layers retain their identities, at least for the dominant rows 1, 3 & 5. The measurements within the patch should be able to shed more light on this.

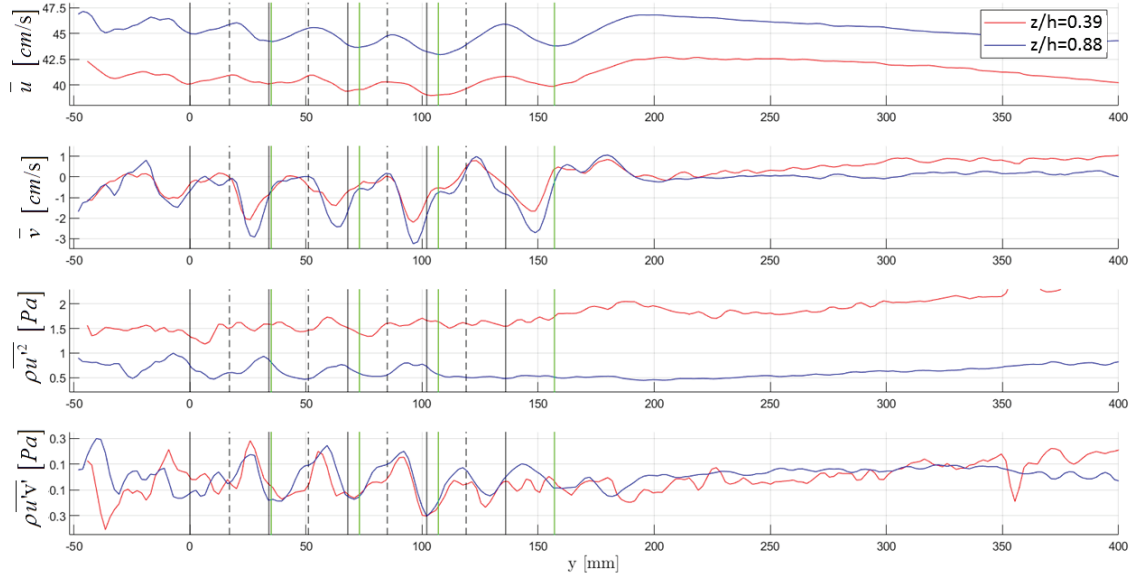


Figure 5. Lateral profiles of the time-averaged longitudinal velocity \bar{u} , the time averaged lateral velocity \bar{v} , the normal turbulent stress $\rho \bar{u}'^2$, the lateral turbulent shear stress $\rho \bar{u}' \bar{v}'$, all at $z/h = 0.39$ and 0.88 . $x = 36.6$ cm, downstream of the patch. The black solid and dashed vertical lines indicate the positions of the glass blades and the green vertical lines indicate the position of the minima of \bar{u} .

The three measurement planes including allow a momentum balance to be performed to estimate the drag exerted on the patch. For a control volume given by the three planes and assuming a hydrostatic pressure distribution at the control surfaces upstream and downstream, the momentum balance over half the patch along the symmetry line writes as:

$$\begin{aligned}
D_x = & -\rho \underbrace{\int_{A_1} \bar{u} \bar{u} dA}_{Adv_1} + \rho \underbrace{\int_{A_3} \bar{u} \bar{u} dA_3}_{Adv_3} + \rho \underbrace{\int_{A_2} \bar{u} \bar{v} dA_2}_{Adv_2} - \rho \underbrace{\int_{A_1} \bar{u}' \bar{u}' dA_1}_{Turb_1} + \rho \underbrace{\int_{A_3} \bar{u}' \bar{u}' dA_3}_{Turb} + \rho \underbrace{\int_{A_2} \bar{u}' \bar{v}' dA_2}_{Turb_2} \\
& - \underbrace{\rho g I \cdot V_{cv}}_{Gravity} - \underbrace{\tau_{bed} A_b}_{Bed Shear Stress} - \underbrace{\rho g B \left(\frac{h_1^2 - h_3^2}{2} \right)}_{Press. Grad}
\end{aligned}$$

Here, D_x is the total force exerted by the blades on the fluid due to viscous and pressure forces (i.e., it should be negative). The indices 1, 2 & 3 of the integration areas A_i and water depths h_i refer the portions of the measurement planes A1, A2 & A3, respectively, which intersect to give the control surface of the control volume V_c . A_b is the surface area of the control volume adjacent to the bed and I is the bed-slope. Bed friction τ_{bed} (here negative) is estimated via the friction velocity measured with the patch and the water depths h_i were determined from the PIV images. Figure 6 shows the resulting terms. It can be seen that the pressure term given by the water depths is the leading order term followed by the net streamwise advection of streamwise momentum across the transverse planes. Momentum loss through the side is about a third as that through the transverse sections but of opposite sign, reducing the drag force which the patch exerts. The turbulent stress terms play no significant role and the gravity term is also small. The drag coefficient defined with the frontal area of the patch $C_D = \frac{-2D_x}{bh_p \rho U_b^2}$, yields $C_D = 0.42$.

The wake analysis suggests that the boundary layers developing on the glass blades dominate the wake. To pursue this, the frictional drag force acting on both sides of the glass blades was estimated with a standard turbulent boundary layer relationship $C_f = 0.032 Re_l^{-1/7}$ with l the length of the blades in Re_l and taking U_b as the reference velocity for simplicity. The resulting frictional force for the half-patch considered in the control volume is -0.38 N, compared to -1.95 N

for $D_{s,i}$, i.e., about 20%. Accordingly, the drag coefficient reduces to $C_D = 0.34$ when subtracting the estimated frictional force exerted by the blades. This suggests that the interaction of the individual wakes plays an important role, more than the direct frictional effects. Of course, the frictional drag estimation also assumes free-stream potential flow and can therefore underestimate the frictional drag.

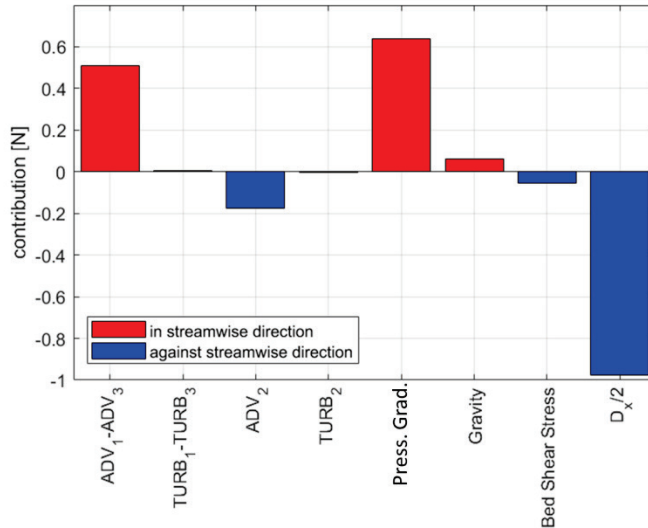


Figure 6. Contribution of the different terms to the drag D_x in the momentum balance.

CONCLUSION

The flow field around a patch made of thin glass plates aligned with the flow was measured via stereoscopic PIV in order to estimate the drag exerted by the patch on the flow. The patch was designed to meet the allometric characteristics of a real leafy floodplain plant (willow), with a leaf-area index (LAI) of 4 and a porosity of 98%. The patch was positioned on a manually-levelled gravel bed and the plates extended up to the free surface ($h/h_p = 1$), while the width of the patch was less than one-tenth of the flume width ($b/B < 10$) to be a shallow water configuration without side-wall effects. Analysis of the longitudinal mean velocity and the lateral turbulent shear stress profiles in the transverse plane of the near wake revealed the signatures of vertically aligned wakes generated by the glass sheets. These wakes appear to interact and to deviate sideways and dominate the wake-behaviour of the patch. In other words, the patch does not generate a single dominant large-scale wake behaviour. The momentum balances yields a drag coefficient of $C_D = 0.42$. A rough estimate of the frictional force acting on the glass plates as if each plate was isolated in uniform and potential flow yields a frictional-resistance to total-drag ratio of 0.2 so that the drag coefficient without this estimated frictional resistance is reduced to 0.34 – still relatively high. This estimate suggests that the pressure losses and interactions between the separating boundary-layer wakes is nevertheless rather significant, despite an LAI of 4 and a porosity of 98%, but needs to be confirmed with measurements and LES simulations within the patch. 2D-PIV data of the flow within the artificial patch should help to elucidate the interaction of the wakes as well as the actual bed shear stress in the presence of the patch. Furthermore, other measured flow velocities and depths still need to be analysed and compared to the real-plant equivalent.

ACKNOWLEDGEMENT

This project has received funding from the European Union's Horizon 2020 research and innovation programme under grant agreement No 654110, HYDRALAB+.

REFERENCES

- Aberle, J., Järvelä, J. (2013). Flow resistance of emergent rigid and flexible flood plain vegetation. *J. Hydr. Res.*, 51(1), S. 33-45.
- Armanini, A., Righetti, M., Grisenti, P. (2005). Direct measurement of vegetation resistance in prototype scale. *J. Hydr. Res.*, 43(5), S. 481-487.
- Bai, K., Meneveau, C., Katz, J. (2012). Near-wake turbulent flow structure and mixinglength downstream of a fractal tree, 143,. *Boundary Layer Met.*, S. 285–308.
- Bai, K., Meneveau, C., Katz, J. (2013). Experimental study of spectral energy fluxes in turbulence generated by a fractal treelike object. *Phys. Fluids*, 25, S. 110810.
- Boothroyd, R.J., Hardy, R.J., Warburton, J., Marjoribanks, T.I. (2015). The importance of accurately representing submerged vegetation morphology in the numerical prediction of complex riverflow. *Earth Surf. Process and Landf.*
- Chang, W.-Y., Constantinescu, G., Tsai, W. F. (2017). On the flow and coherent structures generated by a circular array of rigid emerged cylinders placed in an open channel with flat and deformed bed. *J. Fluid Mech.*, 831, S. 1-40.
- Chen, Z., Ortiz, A., Zong, L., Nepf, H. (2012). The wake structure behind a porous obstruction and its implications for deposition near a finite patch of emergent vegetation. *Water Res. Res.* 48(9).
- Jalonen, J., Järvelä, J., Aberle, J. (2013). Leaf area index as a vegetation density measure for hydraulic analyses. *J. Hydr. Eng.*, 139(5), pp. 461-469.
- Kim, H.S., Kimura, I., Shimizu, Y. (2015). Bed morphological changes around a finite patch of vegetation. *Earth Surf. Process. Landf.*, 40 , S. 375-388.
- Liu, C., Nepf, H. (2016). Sediment deposition within and around a finite patch of model vegetation over a range of channel velocity. *Water Res. Res.*, 52.
- Marjoribanks, T. I., Hardy, R. J., Lane, S. N., Parsons, D. R. (2014). The hydraulic description of vegetated riverchannels: the weaknesses of existing formulations and emerging alternatives. *Wiley Interdisciplinary Reviews: Water* 11/2014, 1(16).
- Marjoribanks, T. I., Hardy, R. J., Lane, S. N., Parsons, D. R. (2014a). High-resolution numerical modelling of flow–vegetation interactions. *J. Hydr. Res.* 52(6), S. 775-793.
- Marjoribanks, T. I., Hardy, R. J., Lane, S. N., Parsons, D. R. (2014b). The hydraulic description of vegetated riverchannels: the weaknesses of existing formulations and emerging alternatives. *Wiley Interdisciplinary Reviews: Water* 11/2014, 1(16).
- Nicolle, A., Eames, I. (2011). Numerical study of flow through and around a circular array of cylinders. *J. Fluid Mech.*, 679, S. 1-31.
- Rominger, J. T., Nepf, H. M. (2011). Flow adjustment and interior flow associated with a rectangular porous obstruction. *J. Fluid Mech.*, 680, S. 636-659.
- Stoesser, T., Kim, S. J., Diplas, P. (2010). Turbulent flow through idealized emergent vegetation. *J. Hydr. Eng.* 136(12), S. 1003–1017.
- Tanino, Y., Nepf, H. M. (2008). Laboratory investigation of mean drag in a random array of rigid emergent cylinders. *J. Hydr. Eng.*, 134(1), S. 34–41.
- Thomas, R.E, McLelland, S.J. (2015). The impact of macroalgae on mean and turbulent flow fields. *J. Hydrodyn.*, 27(3), S. 427-435.
- Wunder, S., Lehmann, B., Nestmann, F. (2011). Determination of the drag coefficients of emergent and just submerged willows. *J. River Basin Management*, 9(3-4), S. 231-236.
- Zong, L., Nepf, H. (2011). Vortex development behind a finite porous obstruction in a channel. *J. Fluid Mech.* 691, S. 368–391.